47
9-13-95 JS ②

PREPARED FOR THE U.S. DEPARTMENT OF ENERGY,
UNDER CONTRACT DE-AC02-76-CHO-3073

PPPL-3125
UC-427

PPPL-3125

NONLINEAR ω*-STABILIZATION OF THE m=1 MODE IN TOKAMAKS

BY

B. ROGERS AND L. ZAKHAROV

AUGUST 1995

PPPL PRINCETON PLASMA PHYSICS LABORATORY

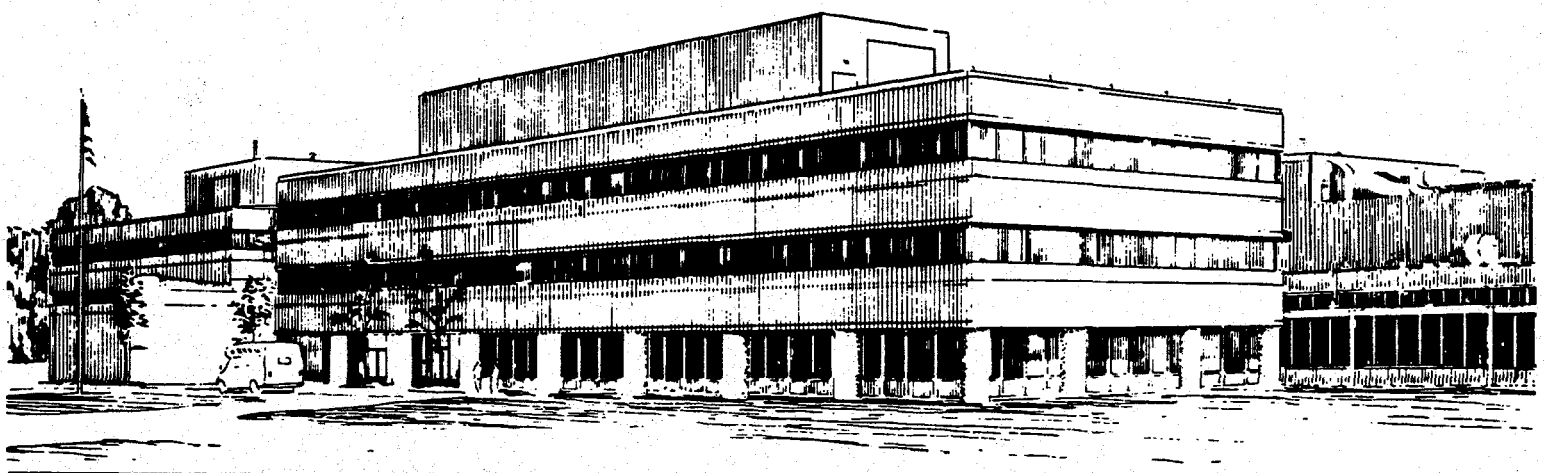

PRINCETON UNIVERSITY, PRINCETON, NEW JERSEY

NOTICE

DISCLAIMER

Portions of this document may be illegible in electronic image products. Images are produced from the best available original document.

Nonlinear ω_*-stabilization of the $m = 1$ mode in tokamaks

B. Rogers

Institute for Plasma Research

University of Maryland

College Park, Maryland 20742-3511

L. Zakharov

Princeton Plasma Physics Laboratory

P.O. Box 451

Princeton, New Jersey, 08543-0451

Abstract

Earlier studies of sawtooth oscillations in Tokamak Fusion Test Reactor supershots (Levinton, *et al*, Phys. Rev. Lett. **72**, 2895 (1994); Zakharov, et al, *Plasma Phys. and Contr. Nucl. Fus. Res., Proc. 15th Int. Conf., Seville 1994*, Vienna) have found an apparent contradiction between conventional linear theory and experiment: even in sawtooth-free discharges, the theory typically predicts instability due to a nearly ideal $m = 1$ mode. Here, the nonlinear evolution of such mode is analyzed using numerical simulations of a two-fluid magnetohydrodynamic (MHD) model. We find the mode saturates nonlinearly at a small amplitude provided the ion and electron drift-frequencies $\omega_{*i,e}$ are somewhat above the linear stability threshold of the collisionless $m = 1$ reconnecting mode. The comparison of the simulation results to $m = 1$ mode activity in TFTR suggests additional, stabilizing

effects outside the present model are also important.

52.35.Py, 52.30.Fb, 52.55.Fa

I. INTRODUCTION

Recent comparisons[1,2] of sawtooth behavior in TFTR[3] (Tokamak Fusion Test Reactor) to theoretical models have revealed an apparent inconsistency: in sawtooth-free, higher-β discharges, conventional linear MHD (Magnetohydrodynamic) stability analysis indicates the presence of an unstable, predominantly ideal $m = 1$ mode.

To determine if this "anomalous stability" will apply to future tokamaks, its origin must be understood. Important progress on this was made in Ref. 1, in which a simple condition was found that reliably determines the sawtooth-free operational space of TFTR in all presently known regimes. This condition is in fact the linear, $m = 1$ mode ω_*-stability condition of the two-fluid model in a certain limit. The limit corresponds to the collisionless reconnecting mode and may be defined in terms of three essential scale-lengths in the two-fluid model: the ideal mode layer-width[4] $\lambda_h \simeq \sqrt{3}\pi r_1^2(\beta_p^2 - (0.3)^2)/(q_1' R^2)$ (related to the ideal MHD $m = 1$ growth rate by $\lambda_h = \gamma\tau_A/(r_1 q_1')$ with $\tau_A = R/V_A|_{r_1}$, so $\lambda_h > 0$ indicates instability); the ion-sound Larmor radius $\rho_s = \sqrt{(T_e + T_i)/m_i\Omega_{ci}^2}$ (arising from finite parallel electron compressibility); and the collisionless skin depth $d_e = c/\omega_{pe}$ (due to electron inertia in Ohm's law, which is dominant over resistivity in TFTR). The collisionless reconnecting mode limit is $|\lambda_h| \ll \rho_s, d_e$, i.e., the case in which the ideal MHD driving term λ_h is negligible compared to the destabilizing collisionless effects associated with ρ_s and d_e. The contradiction with experimental analysis is that typical supershot discharges seem to correspond to the opposite case, $\lambda_h > \rho_s, d_e$, in which the linear mode is unstable and predominantly ideal. The results from linear theory in these two limits are now considered in detail.

For either ordering of λ_h, ρ_s, and d_e the two-fluid model predicts the $m = 1$ mode can be linearly stabilized by sufficiently large values of $\omega_{*j} = -cp_j'/(nq_j rB)|_{r_1}$, $j = i, e$. For example, taking the case of $T_i \gg T_e$ and isothermal ions, the stability condition is $\omega_{*i}/2 > \gamma_0$, where γ_0 is the growth rate of the mode for $\omega_{*j} = 0$. For typical TFTR supershot values, $\lambda_h \sim 1 - 2$ cm, $\rho_s \sim 0.5$ cm, $d_e \sim 0.08$ cm, one obtains (as discussed later)

$\gamma_0\tau_A \simeq q_1'\sqrt{\lambda_h^2 + (\rho_s^2 + 5d_e^2)/2}$ ($> q_1'\lambda_h$). For $\lambda_h = 0$ (and $\rho_s > d_e$), on the other hand, γ_0 is given by[5] $\gamma_0\tau_A \simeq q_1'\rho_s[2d_e/(\rho_s\pi)]^{1/3}$ ($< q_1'\rho_s$). Since $\lambda_h > \rho_s$, a range of ω_* values therefore exists in which the former expression for γ_0 leads to a prediction instability while the latter does not, and it is in such a range that the apparent violation of linear theory cited above occurs.

In summary, when λ_h is calculated for typical TFTR supershots (such as those discussed in Ref. 1), it is so large that linear MHD stability analysis cannot account for the observed periods of sawtooth-free operation with $q(0) < 1$. In particular, it is so large that the stability condition found in Ref. 1, which is based on $\lambda_h = 0$, cannot be justified in the context of linear theory. The agreement of that condition with experiment therefore needs further explanation.

A possible resolution of this problem is that effects outside the two-fluid model thus far considered effectively reduce the value of λ_h. For example, trapped energetic[6] and thermal[7] particles can have such an influence. Studies[1,8] of the former effect, however, have found it alone to be insufficient to explain the experimental results. Similarly, linear stabilization by the latter is problematic[7] due to the usual disparity between T_i and T_e (e.g., $T_i > 2T_e$) in TFTR. At a more basic level, these effects, while apparently important quantitatively, seem too small to account for the observed stability in at least the more extreme cases.

Here, we follow the assumption that such stabilizing effects are absent or insufficient, and address the proposal of Ref. 2 that nonlinear ω_* effects lead to the observed sawtooth-stability condition. Such an explanation is in fact consistent with[2] the common observation in TFTR of a saturated, nonlinear $m = 1$ mode. Considering a linearly unstable parameter regime like that of TFTR described above, we present numerical simulations of a reduced two-fluid model that determine the early nonlinear evolution of the mode for various values of $\omega_{*i,e}$.

The application of a reduced MHD model to a cylindrical geometry, like that previously considered in studies of the $m = 1$ mode,[9,10] cannot address this problem, since the ideal

$m = 1$ mode in such a system is neutrally stable. The early nonlinear stage of interest here, though, may be analyzed using a more efficient approach. Following the standard boundary layer decomposition of linear and early-nonlinear[11,12] $m = 1$ mode theory, the reduced two-fluid equations are solved numerically in a narrow "layer region" ($|r - r_1| \ll r_1$) surrounding the $q = 1$ surface which includes the reconnection layer and $m = 1$ island only – see Fig. 1; the external regions are represented by the usual boundary condition appropriate to an arbitrary, specified Δ'_m-spectrum. Curvature is neglected in the layer region, which is described in a Cartesian geometry. The parameter λ_h, which is related to Δ'_1 by $\lambda_h = -\pi/\Delta'_1$, thus enters through the boundary condition.

To summarize the result, we find the linearly unstable mode indeed saturates, aside from a very slow diffusive evolution on a timescale $\tau > 100/\gamma_{lin}$ (possibly outside the model's scope of physical validity), at a small, ω_*-dependent amplitude, provided $\omega_{*i,e}$ are somewhat above the reconnecting mode stability threshold. The main stabilizing effects are nonlinear/quasilinear enhancements near $r = r_1$ of ω_* (i.e., in the present isothermal model, $p' \propto n'$) and the magnetic shear q'. The latter change is also found to weaken the ideal mode contributions relative to those of the reconnecting mode. A nonlinearly/quasilinearly generated, sheared flow layer along $r = r_1$ is also observed. This flow, caused primarily by ion-gyroviscosity, is in the ion diamagnetic drift direction at the center of the layer, but reverses in the layer's outer regions so that the net flow is zero. Its effect is stabilizing, but at a generally weaker level.

At least at smaller saturation amplitudes, these effects are well described by a quasilinear analysis of the $|m| = 1$ and $m = 0$ poloidal harmonics. In the case of the density, for example, the nonlinear steepening is then a consequence of $Dn/Dt \simeq 0$, or equivalently, the density continuity equation $\dot{n} = -\nabla \cdot n\mathbf{V}$ with $\nabla \cdot \mathbf{V} \simeq 0$. Averaging the latter form over θ in polar coordinates gives an evolution equation for n_0, the $m = 0$ component of n: $\dot{n}_0 = -(1/r)\partial_r(r\langle nV_r\rangle_\theta) \simeq -\partial_x\langle nV_r\rangle_\theta$, $x = r - r_1 \ll r_1$. Expanding n and V_r as $n = n_0 + n_1 e^{i\theta} + n_1^* e^{-i\theta}$, $V = V_{r1}e^{i\theta} + V_{r1}^* e^{-i\theta}$, this becomes $\dot{n}_0 \simeq -2\mathrm{Re}[\partial_x(n_1 V_{r1}^*)]$. The perturbations n_1 and V_{r1}, with $\dot{n}_1 \simeq \gamma n_1$, are related by the $m = 1$ component of $Dn/Dt = 0$

as $n_1 = -n_{0,x}V_{r1}/\gamma$ (where $n_{0,x} \equiv \partial_x n_0$). Thus, $\dot{n}_0 \simeq 2\gamma_r \partial_x(n_{0,x}|V_{r1}/\gamma|^2)$, or with $n_0 \simeq n^{(0)} + \tilde{n}_0$ for some equilibrium profile $n^{(0)}(x)$, $\tilde{n}_0 \simeq \partial_x(n^{(0)}_{,x}|V_{r1}/\gamma|^2)$. Given the ideal MHD result (valid even for $\omega_* \neq 0$ - see the Appendix) $|V_{r1}/\gamma|^2 = (\xi_0^2/(4\pi^2))\left(\tan^{-1}(x/\lambda_h)\right)^2$, where ξ_0 is shift of the plasma core, it is seen that quasilinear effects steepen the equilibrium profile near $x = 0$ as $n_{0,x}(0) = n^{(0)}_{,x}(0)[1 + \xi_0^2/(2\lambda_h^2\pi^2)]$. Similar results for the helical flux ψ and the stream function ϕ are obtained in the ideal case from Ohm's law and the vorticity equation: $\tilde{\psi}_0 \simeq \partial_x(\psi^{(0)}_{,x}|V_{r1}/\gamma|^2)$ and $\phi_0 = (T_i/2)\tilde{n}_0$.

We emphasize that the stabilizing contribution from ω_* (i.e., $n^{(0)}_{,x}$ in the above argument) is essential for the nonlinear saturation of the mode. This is not the case in the one-fluid, ideal MHD limit $d_e = \eta = \rho_s = 0$, $\omega_* = 0$, in which the ideal $m = 1$ mode saturates at a finite displacement $\xi_0 \sim 4.4\lambda_h$ due to nonlinear changes in ψ alone.[11] This stability is lost, however, in the presence non-ideal effects such as d_e, which allow magnetic reconnection to take place and thus permit continued growth of the mode, e.g.,[13] $\xi_0 \simeq .54w$ for a given $m = 1$ island width $w \gg \lambda_h$. As described above, in the presence of ω_* the nonlinear saturation can be regained at an amplitude which, depending on ω_*, can be smaller or larger than the ideal MHD value. In contrast to the ideal case, furthermore, the current layer near $r = r_1$ in the saturated state is nonsingular.

II. TWO-FLUID MODEL

We consider a reduced two-fluid model describing the evolution of the (normalized) velocity stream function ϕ, helical flux ψ, and electron pressure p:

$$\dot{W} + \mathbf{V} \cdot \nabla W - \tau \nabla \cdot [p, \nabla\phi] = -\mathbf{B}_* \cdot \nabla J + \mu \nabla^2 W, \tag{1}$$

$$\dot{\psi} + \mathbf{B}_* \cdot \nabla(\phi - (1+\tau)p) = \eta J + d_e^2 \left(\dot{J} + [\phi - \tau p, J] - \mu_e \nabla^2 J\right), \tag{2}$$

$$\dot{p} + \mathbf{V} \cdot \nabla p = -\left(\rho_s^2/(1+\tau)\right)\mathbf{B}_* \cdot \nabla J + \kappa \nabla^2 p, \tag{3}$$

Definitions (with toroidal unit vector $\hat{y} = -\hat{\zeta}$):

$$\mathbf{B}_* = -\hat{y} \times \nabla\psi \ , \quad \mathbf{V} = \hat{y} \times \nabla\phi \ , \quad [a,b] = \hat{y} \cdot \nabla a \times \nabla b,$$

$$J = \nabla^2\psi \ , \quad W = \nabla^2\phi \ , \quad \tau = T_i/T_e,$$

$$1/\tau_A^* = (q'rV_A/R)_{r=r_1} \ , \quad 1/\tau_r = c^2\eta_{||}/(4\pi r_1^2) \ , \quad \eta = \tau_A^*/\tau_r,$$

Normalizations (normalized $\rightarrow$ physical units):

$$\rho_s \rightarrow \rho_s/r_1 \ , \quad d_e \rightarrow d_e/r_1 \ , \quad \lambda_h \rightarrow \lambda_h/r_1 \ , \quad \text{etc.}$$

$$t \rightarrow t/\tau_A^* \ , \quad \omega_{*i,e} \rightarrow \omega_{*i,e}\tau_A^* \ , \quad \text{etc.}$$

$$\phi \rightarrow (\tau_A^*/r_1^2)\phi \ , \quad \psi \rightarrow (R/[r_1^2 q_1' B])\psi \ , \quad p \rightarrow (\tau_A^*\omega_{*e}/p_1')(p - p_1),$$

Here, length and time scales are normalized to r_1 and $\tau_A^* = \tau_A/(r_1 q_1')$, respectively, where the constants q_1', ω_{*e}, p_1, p_1', etc., refer to the unperturbed tokamak equilibrium. (In TRTR, $r_1 \sim 20 - 30$ cm, $\tau_A^* \sim 5 \times 10^{-7}$ sec.) This is a simplified version of the four-field model of Hazeltine et al.[14]. Since our main goal here is to demonstrate the basic phenomena, we have omitted for simplicity (as in Ref. 15) various effects that we expect to have a quantitative but secondary role: the toroidal curvature terms, some finite ion Larmor radius terms $\propto \rho_i^2\nabla^2$, and the parallel ion velocity terms. In the linear $m = 1$ mode limit, these equations correctly reproduce the ω_* factors obtained from more detailed two-fluid and kinetic treatments (e.g., Refs. 5 and 16), given the implicit assumption of constant T_i, T_e.

The diffusion terms $\propto \mu, \mu_e, \kappa$ represent[9,10,17] effective ion and electron perpendicular viscosity (μ, μ_e) and anomalous particle diffusion (κ). The role of μ_e in the simulations deserves further comment. For $\mu_e = 0$ and $d_e > \eta^{1/3}$, two-dimensional models like the above[17,18] generate exponentially small, sub-d_e structure in the nonlinear current layer. This behavior is probably unphysical, as three-dimensional studies[19] have found such structure to be broadened by current density gradient driven instabilities. In any event, the total

current associated with this structure is negligible, as is its effect on the global dynamics of our system. Here, the μ_e term acts to suppress such sub-d_e scale-length features.

The code used here to analyze this model is a suitably modified version of that described in Ref. 17. The equations are solved on a Cartesian grid $n_x \times n_z$, $n_x = 205$, $128 \leq n_z \leq 256$, with a variable grid-spacing in the x-direction.

A. Asymptotic Matching to Linear Ideal Solution

The layer region can be described using a Cartesian, layer-centered coordinate system (x, z), with radial coordinate x, helical coordinate z (i.e., $z \simeq \theta - \zeta$ with θ and ζ being the poloidal and toroidal angles, respectively), and periodic boundary conditions in z. Some explanation is needed regarding the definition of x. As the $m = 1$ mode evolves nonlinearly, flux surfaces near the central core are shifted rigidly some finite distance $\xi_0(t)$. To maintain force balance in the early nonlinear stage ($\xi_0 \ll r_1$), the effective $q = 1$ surface – i.e., the axis of the reconnection layer and island – is shifted half this distance,[20,13] and may be defined for example by $|\mathbf{r}| \simeq \bar{r}_1$, $\bar{r}_1 = r_1 + \xi_0 \cos(\theta - \zeta)/2$. This shift also preserves the (approximate) symmetry of the helical flux and pressure gradient across the layer region. Therefore, defining x as the radial distance from the shifted $q = 1$ surface as $x \simeq (r - \bar{r}_1)/r_1$, one may apply even x-parity boundary conditions on ψ, p' and ϕ' at the edge of the layer region. The resulting definite parity solutions can be obtained from a simulation of only the half-space $x \geq 0$, with appropriate "reflecting" boundary conditions at $x = 0$.

The x-boundary condition on the potentials can be applied at an arbitrary value $|x| = x_l$ satisfying $w/r_1 << x_l << 1$ (here, typically, $x_l \sim 0.3$). It is based on linear theory and the $x \to 0$ forms of the equilibrium profiles, taken as

$$\phi^{(0)} = 0 \tag{4}$$

$$\psi^{(0)} = (\cos(k_x x) - 1)/k_x^2 \simeq -x^2/2 + k_x^2 x^4/4! + \ldots \tag{5}$$

$$p^{(0)} = \omega_{*e} x \tag{6}$$

for given constants ω_{*e} $(= \tau_A^* \omega_{*e})$, k_x. As expected, the simulations are insensitive to the choice of k_x for $k_x \sim 1$ or smaller (e.g., $k_x \to 0$ and $k_x = 1$ yield nearly equivalent results). Note the electric potential is related to ϕ by $\phi_{elec} = \phi - \tau p$, so for $\tau \neq 0$ the above implies an equilibrium, uniform radial electric field E_x of magnitude $\tau\omega_{*e} = -\omega_{*i}$. This results in no loss of generality, as other values of $E_x \to E_x - V_0$ are obtained with the transformation $y \to y - V_0 t$.

Neglecting the inertia terms in Eq. (1) for $x \sim x_l$, ψ obeys $\mathbf{B}_* \cdot \nabla J \approx 0$, which leads to the conventional "exterior" linear solution for $\tilde{\psi} = \psi - \psi^{(0)}$:

$$\tilde{\psi} = \sum_m \tilde{\psi}_m e^{imz} \ , \quad \tilde{\psi}_m \approx c_m \left(|x| + 2/\Delta'_m \right) \ , \quad \Delta'_m = \left[\frac{\tilde{\psi}_{m,x}}{\tilde{\psi}_m} \right]_{x \to 0-}^{x \to 0+} \tag{7}$$

for some c_m and a specified set $\{\Delta'_m\}$. In detail,

$$\mathbf{B}_* \cdot \nabla J = [J, \psi] \simeq \psi^{(0)}_{,x} \sum_m im \left(\tilde{\psi}_{m,xx} + k_m^2 \tilde{\psi}_m \right) = 0 \ , \quad k_m^2 = k_x^2 - m^2 \tag{8}$$

so $\tilde{\psi}_m$ may be written as

$$\tilde{\psi}_m(x) = \tilde{\psi}_m(x_l) \frac{f_m(x)}{f_m(x_l)} \tag{9}$$

where

$$f_m(x) = \frac{1}{k_m} \sinh(|k_m x|) + \frac{2}{\Delta'_m} \cosh(|k_m x|) \qquad (k_m^2 > 0) \tag{10}$$

$$= \frac{1}{|k_m|} \sin(|k_m x|) + \frac{2}{\Delta'_m} \cos(|k_m x|) \qquad (k_m^2 < 0) \tag{11}$$

$$= |x| + 2/\Delta'_m \qquad (k_m x \to 0) \tag{12}$$

As a result,

$$\nabla^2 \psi = -k_x^2 \psi - 1 \ , \quad [J, \psi] = 0 \tag{13}$$

are satisfied exactly. Similar asymptotic forms for ϕ and p follow from the linearized versions of Eqs. (2) and (3) (neglecting the small diffusion, ρ_s, and d_e terms):

$$\phi_m(x) = \phi_m(x_l) \frac{\sin(k_x x_l)}{\sin(k_x x)} \frac{f_m(x)}{f_m(x_l)} \tag{14}$$

$$\tilde{p}_m(x) = \tilde{p}_m(x_l) \frac{\sin(k_x x_l)}{\sin(k_x x)} \frac{f_m(x)}{f_m(x_l)} \tag{15}$$

Linear theory clearly does not determine the amplitudes of the potentials at $x = x_l$. Rather, these amplitudes are determined by Fourier analysis at a given time in the simulation. The above asymptotic forms are then used to compute the various x-derivatives that are needed to advance the potentials to the next timestep near $x = x_l$.

We consider a Δ'_m-spectrum appropriate to a tokamak, e.g., $\Delta'_1 = -\pi/\lambda_h \sim (R/r_1)^2$ and, for $|m| \neq 1$, $\Delta'_m \sim -1$. The initial perturbation is chosen to have an $|m| = 1$ component only. Near the edge of simulation where the boundary condition is applied, the $|m| = 1$ component remains much larger than the other components throughout the entire simulation. Consequently, the results are insensitive to the values of Δ'_m for $|m| \neq 1$. For $|m| \gg 1$, however, to avoid numerical instability, it is necessary to choose $\Delta'_m = -2k_m$, which eliminates the growing exponential in Eq. (10).

III. SIMULATION RESULTS

Simulations have been carried out in a parameter range relevant to future and present tokamaks (TFTR in particular) which is linearly unstable to a predominantly ideal $m = 1$ mode; a typical case, referred to below, is

$$\lambda_h = .03\ , \quad \rho_s = \tfrac{1}{2}\lambda_h = .015\ , \quad d_e = \tfrac{1}{3}\lambda_h = .01\ , \quad \tau = 1 \tag{16}$$

$$\eta = 10^{-9}\ , \quad \mu = \mu_e = \kappa = 5 \times 10^{-7} \tag{17}$$

That is, λ_h $(= \lambda_h/r_1)$ is positive and larger than the collisionless scale lengths ρ_s and d_e. (Here, d_e is 2–3 times larger than realistic TFTR values.) These effects are dominant over the diffusive terms $\propto \eta$, μ, μ_e, κ, which modify the linear eigenfrequency by only a few percent. Various values of ω_* are considered, all of which are insufficient to stabilize the mode linearly (ignoring, that is, the diffusive terms, which can typically lead to weak instabilities for any ω_*).

A useful diagnostic of the mode's evolution is the maximum displacement of a flux surface, $\xi(t)$, relative to its initial x-position far from the singular layer, $x \gg \lambda_h$. Referring to the

lab frame $\xi_0(t) = 2\xi(t)$, where ξ_0 is the core displacement discussed earlier. Shown in Fig. 2 are the results of two simulations, which differ only in the values of ω_*: in one $\omega_{*i} = \omega_{*e} = 0$, while $\omega_{*i} = -\omega_{*e} = .054 = 1.8\lambda_h$ in the other. Both cases are linearly unstable, although the growth rate in the second (γ_r $(= \tau_A^* \gamma_r) \simeq 0.017$) is reduced relative to the $\omega_* = 0$ value ($\gamma \simeq 0.036$) by roughly 50%.

The mode in the $\omega_* \neq 0$ case does not completely saturate nonlinearly; rather, the amplitude continues to grow slowly after it reaches an initial maximum. Such residual, slow evolution results from the small diffusive terms $\propto \mu_e, \kappa, \mu$ which are necessarily included in the model at some level for numerical reasons. This is illustrated in Fig. 3, which shows $\xi(t)$ for the same parameters as the $\omega_* \neq 0$ case in Fig. 2 except $\mu_e = \kappa = \mu = 3 \times 10^{-6}$ (a factor of six increase). The resulting increase in the slow growth is consistent with a scaling, e.g., $\tau_{slow} \propto \mu_e^{-p}$, $1/3 < p < 1/2$ (further simulations indicate μ here has a stabilizing effect). Such behavior may be related to the claim of Ref. 9 that the resistive mode does not completely saturate for $|\omega_{*e}| < \gamma_{lin}$.

The approximate saturation amplitudes obtained from the simulations for various ω_* values are plotted in Fig. 4. In the simulations marked by asterisk symbols, the parameters, aside from ω_* and $\mu = \mu_e = \kappa = 10^{-6}$, are the same as in Fig. 2. The triangles represent an increase in $\tau = T_i/T_e$ by a factor of three, i.e., $T_e = T_i/3$. The squares, also with $T_e = T_i/3$, indicate the result of doubling ρ_s, i.e., $\rho_s = 0.03 = \lambda_h$. In all cases, the symbols correspond to the ξ-values at which $\ddot{\xi}$ first passes through zero. These values are insensitive to changes in the small diffusion terms, and are typically about 25% smaller than the first maximum of ξ. In Figs. 2 and 3, for example, $\ddot{\xi} = 0$ at $t = 355$ and $t = 378$, respectively, where ξ $(= \xi/r_1) \simeq 0.039$ in both cases.

The amplitudes for the larger ω_{*i} values fall below that expected in the ideal MHD case ($\xi \simeq 2.2\lambda_h$), with larger, unshown ω_{*i} values leading to smaller amplitudes until linear stability is reached. The linear, reconnecting mode stability boundary discussed in Ref. 1 can be represented in Fig. 4, for each of the three cases shown, as a vertical line at a particular ω_* value. (For example, for $T_i = T_e$ and $\rho_s \gg d_e$, the marginal stability condition

is[5] ω_{*i} $(= \omega_{*i}\tau_{A*}) = (\rho_s/r_1)[2d_e/(\rho_s\pi)]^{1/3}$, with larger ω_* being stable.) Normalizing these marginal ω_* values to the value of λ_h in the simulations ($\lambda_h/r_1 = 0.03$), one finds $\omega_{*i}/\lambda_h \simeq 0.5$ (asterisks), 0.7 (triangles), 0.9 (squares). It is seen that the amplitudes increase more rapidly as these limits are approached. Due to the restriction $\xi/r_1 \ll 1$, the largest amplitudes shown are about $0.12r_1$, which occurs for ω_{*i}/λ_h about $40-50\%$ above the respective reconnecting mode threshold. Thus, for the considered parameters, there is a substantial "gap" between the latter threshold and the region of early-nonlinear stability. This may indicate additional stabilizing factors, such as the trapped particle effects mentioned earlier, are important.

The contributions of ω_{*i} and ω_{*e} to the *linear*, $\lambda_h = 0$ stability boundary are comparable (see, e.g., Ref. 16). As can be seen from the scaling of the nonlinear amplitudes with τ, the same is generally true nonlinearly. At the larger ω_{*i} values with $\rho_s = \lambda_h/2$ (asterisks, triangles), however, the contribution of ω_{*e}, relative to ω_{*i}, weakens. As discussed below, ω_{*e} enters the linear and quasilinear theory only though the non-ideal terms, which (for the $\rho_s < \lambda_h$ cases) are overwhelmed by ideal effects at larger ω_{*i}. Also, the larger amplitudes of the two $T_e = T_i/3$ cases (triangles: $\rho_s = 0.015$, squares: $\rho_s = 0.03$) tend to converge, indicating the influence of ρ_s becomes weaker.

Referring to the $\omega_* \neq 0$ simulation of Fig. 2, Figs. 5a,b show equally spaced contours of the helical flux ψ and current J at the time $t = 400$ of the first maximum of ξ ($\xi \simeq -.054 = 1.8\lambda_h$ - a typical value). The saturated configuration contains an $m = 1$ island of half-width $w/2 \sim \xi$ and angular extent (excluding the current layer) $\Delta\theta \sim \pi$. At larger ξ/λ_h values, the island proportions increase, gradually approaching the $\lambda_h = 0$ prediction[13] $w/2 \sim 2\xi$, $\Delta\theta \sim 4\pi/3$.

At this same time ($t = 400$), Figs. 6a-c show Fourier analyses of ϕ, $p - p^{(0)}$, $\psi - \psi^{(0)}$. The $m = \pm 1$ components are dominant, followed in magnitude by the perturbation in the $m = 0$ component, followed by $m = \pm 2$, etc. (Since the potentials are real, $\psi_{-m} = \psi_m^*$, etc., so for $m \neq 0$ we plot $|\psi_m| + |\psi_{-m}| = 2|\psi_m|$ rather than $|\psi_m|$.) To clarify the saturation mechanism we therefore consider the quasilinear analysis of the $|m| = 1$ mode, retaining quasilinear

corrections from the $m = 0$ mode only. We show below these $m = 0$ corrections alone—particularly those in p and ψ— can account for the saturation in the simulations. They represent nonlinear enhancements of the pressure gradient, magnetic shear, and poloidal flow, near $r = r_1$. Due to the weakness of the mode from the MHD viewpoint, these changes are small compared to the equilibrium profiles. This is demonstrated by Figs. 7a-c (solid lines), which show the full $m = 0$ harmonic of ϕ', p', and ψ' at $t = 400$, compared to the initial, unperturbed profiles (dashed lines). In physical units, $\phi' \to -(\tau_A^*/r_1)V_z$, $p' \to (\omega_{*e}\tau_A^*/p_1')p'$, $\psi' \to (1-q)/(q_1'r_1)$. Figure 7a therefore implies $V_z(x=0) \sim 0.03 r_1/\tau_A^* \sim \omega_* r_1$, i.e., a localized flow approaching the ω_*-velocity.

A. Quasilinear Theory

Following a standard approach[21,22,15,16] described in the Appendix, the $m = 1$ components of Eqs. (1)-(3), neglecting all other harmonics except $m = 0$, may be combined to yield a single differential equation obeyed by ϕ_1. We take ϕ_1, ψ_1, $p_1 \propto \exp(\int^t \gamma(t)dt)$, and consider ϕ_0, ψ_0, p_0 for now to be arbitrary functions of x which vary slowly in time relative to γ^{-1}. Also, for simplicity, we neglect the diffusive terms $\propto \mu$, μ_e, κ, and some terms $\propto (\rho_s/\lambda_h)^4$ that vanish in the linear theory limit (i.e., arise from quasilinear corrections only)—see the Appendix. Defining

$$Z = \partial_x (\phi_1/\Gamma) \ , \quad \Gamma = \gamma - i\phi_0' \tag{18}$$

one finds Z obeys

$$Z = \left(\frac{2\lambda_h}{\pi}\int_0^\infty Z dx\right)\frac{1}{D} + \frac{\psi_{0,x}^2}{D}\partial_x\left(\Lambda^2\partial_x\left(\lambda^2 Z\right)\right), \tag{19}$$

where

$$D = \psi_{0,x}^2 + \lambda^2 \ , \quad \lambda^2 = \Gamma(\Gamma - i\Omega_{*i}) \ , \quad \Omega_{*i} = -\tau\Omega_{*e} = -\tau p_0', \tag{20}$$

$$\Lambda^2 = \frac{\lambda_e^2}{\psi_{0,x}^2} + \frac{\lambda_s^2}{\lambda^2} \ , \quad \lambda_s^2 = \frac{\rho_s^2(\Gamma - i\Omega_{*i})}{\Gamma + i(\Omega_{*e} - \Omega_{*i})} \ , \quad \lambda_e^2 = \frac{d_e^2(\Gamma - i\Omega_{*i}) + \eta}{\Gamma + i(\Omega_{*e} - \Omega_{*i})}. \tag{21}$$

Assuming $\psi_0 = \psi^{(0)}$, $p_0 = p^{(0)}$, etc. the above reduces to usual linear theory result.

In the case $\lambda_h^2 \gg \rho_s^2,\ d_e^2$, one can obtain an iterative solution to Eq. (19) in powers of $(\rho_s/\lambda_h)^2$, $(d_e/\lambda_h)^2$:

$$Z = Z^{(0)} + Z^{(1)} + Z^{(2)} + \dots\ , \quad Z^{(0)} = \left(\frac{2\lambda_h}{\pi}\int_0^\infty Z dx\right)\frac{1}{D}. \tag{22}$$

To first order in $\rho_s^2/\lambda_h^2,\ d_e^2/\lambda_h^2$, Z can be replaced by $Z^{(0)}$ in Λ^2-term of Eq. (19):

$$Z = \left(\frac{2\lambda_h}{\pi}\int_0^\infty Z dx\right)\left(\frac{1}{D} + \frac{\psi_{0,x}^2}{D}\partial_x\left(\Lambda^2\partial_x\left(\frac{\lambda^2}{D}\right)\right)\right) + \dots, \tag{23}$$

which, integrating from $(0,\infty)$, leads to the approximate dispersion relation:

$$1 = \frac{2\lambda_h}{\pi}\int_0^\infty \left[\frac{1}{D} + \Lambda^2\left(\partial_x\left(\frac{\lambda^2}{D}\right)\right)^2\right] dx. \tag{24}$$

Neglecting quasilinear corrections (and taking $k_x = 0$), this equation leads the linear theory result $\lambda^2 = \lambda_h^2 + (\lambda_s^2 + 5\lambda_e^2)/2$, which agrees with Ref. 23 as it should for $\rho_s = 0$ and yields (complex) values of γ that agree well with the simulation results in the linear phase.

We now turn to the calculation of the perturbation in the $m = 0$ harmonic. This perturbation, like the $|m| \geq 2$ harmonics, is generated by nonlinear interactions of the $m = \pm 1$ modes. Taking the $m = 0$ moment of Eqs. (1)-(3), for example, neglecting $|m| \geq 2$, one obtains (with $\nabla^2 \simeq \partial_x^2$):

$$\dot{\phi}_0 = 2\mathrm{Im}\left[(\phi_1 - \tau \mathrm{p}_1)\phi_{1,\mathrm{x}}^* + \psi_{1,\mathrm{x}}\psi_1^*\right], \tag{25}$$

$$\dot{\psi}_{e0} = 2\partial_x \mathrm{Im}\left[(\phi_1 - \tau \mathrm{p}_1)\psi_{e1}^* + \mathrm{p}_1\psi_1^*\right]\ , \quad \psi_e = \psi - \mathrm{d}_e^2\psi_{,\mathrm{xx}}, \tag{26}$$

$$\dot{p}_0 = 2\partial_x \mathrm{Im}\left[\phi_1 \mathrm{p}_1^* + \frac{\rho_s^2}{(1+\tau)}\psi_{1,\mathrm{xx}}\psi_1^*\right]. \tag{27}$$

To leading (i.e., quadratic) order in the $m = 1$ amplitude $\sim \xi$, the quasilinear corrections in the $m = 1$ eigenfunctions on the right-hand side (RHS) may be neglected. For $\lambda_h^2 \gg \rho_s^2, d_e^2$, therefore, the leading order results for ϕ_0, $\tilde{\psi}_0$, $\tilde{p}_0$ are obtained by substituting the ideal, linear $m = 1$ eigenfunctions, e.g., $Z^{(0)}$ with $\psi_{0,x} = -x$, $p_{0,x} = \omega_{*e}$, etc., into the RHS, which gives

$$\phi_0 = -(\omega_{*i}/2)\partial_x|\phi_1/\Gamma|^2\ , \quad \tilde{p}_0 = \omega_{*e}\partial_x|\phi_1/\Gamma|^2\ , \quad \tilde{\psi}_0 = -\partial_x\left(x|\phi_1/\Gamma|^2\right), \tag{28}$$

where

$$|\phi_1/\Gamma|^2 = \left(\xi^2/\pi^2\right)\left(\tan^{-1}(x/\lambda_h)\right)^2. \tag{29}$$

It is seen from Figs. (8a-c) that these are in reasonable agreement with the simulation results.

Returning to the dispersion relation, it is now possible to compute the quasilinear eigenvalue γ. We consider here only the simplest case in which η (in addition to μ_e, κ and μ) is neglected. As in the linear theory, in that case (and only in that case) real solutions for $\omega = -i\gamma$ can exist, and one can calculate a stability boundary $\xi_s(\omega_{*j})$, which is the value of ξ for a given ω_{*j} at which a real solution for ω first appears. Larger values of ξ are stable.

The result obtained from Eq. (24) for $\tau = 1$ is shown as the dashed line in Fig. (4). Instead of the lowest order expressions of Eq. (28), slightly more refined versions of ϕ_0, $\tilde{\psi}_0$, $\tilde{p}_0$ were used that account for the ρ_s, d_e corrections to the $m = 1$ linear eigenfunctions. This modification, however, makes only a small change in the final answer. The deviation of the analytic result from the simulation values at smaller ω_{*i} probably indicates the progressive breakdown of the perturbative treatment underlying Eqs. (23) and (24).

Due to the localization of $Z \propto \phi_1'$ near $x = 0$, a qualitative understanding of the saturation behavior may be obtained from Eq. (19) with the estimates

$$\phi_{0,x}(x) \simeq \phi_{0,x}(0) = \chi^2\omega_{*e}\ , \quad \chi = \xi/(\pi\lambda_h), \tag{30}$$

$$p_{0,x}(x) \simeq p_{0,x}(0) = \alpha\omega_{*e}\ , \quad \alpha = 1 + 2\chi^2, \tag{31}$$

$$\psi_{0,x}(x) \simeq \psi_{0,xx}(0)x = -\bar{q}'x\ , \quad \bar{q}' = 1 + 6\chi^2. \tag{32}$$

Also taking $\lambda^2 \simeq \lambda^2(0)$ for simplicity, Eq. (19) can then be written in a form which is identical to the linear theory result with "renormalized" parameters. For example, the quasilinear corrections associated with ϕ_0 and p_0 lead to $\gamma \to \Gamma(0) = \gamma - i\chi^2\omega_{*e}$ and $\omega_{*i,e} \to \Omega_{*i,e}(0) = \alpha\omega_{*i,e}$. Similarly, the quasilinear shear parameter $\bar{q}'$ (which is related to the physical, perturbed shear as $(q_1')_{\xi\neq 0} = \bar{q}'(q_1')_{\xi=0}$) is accounted for by the additional substitutions:

$$\lambda^2 \to \lambda^2/\bar{q}'^2\ , \quad \lambda_h \to \lambda_h/\bar{q}'^2. \tag{33}$$

The linear dispersion relation mentioned above, for example, is therefore modified as $\lambda^2/\bar{q}'^2 = \lambda_h^2/\bar{q}'^4 + (\lambda_s^2 + 5\lambda_e^2)/2$, which, in the simplest case $\omega_{*i} \gg \omega_{*e}$, leads to the stability condition

$$(\alpha/\bar{q}')\omega_{*i} > 2\sqrt{\lambda_h^2/\bar{q}'^4 + (\rho_s^2 + 5d_e^2)/2}. \tag{34}$$

Note the quasilinear enhancement of the shear ($\bar{q}' > 1$) has a net stabilizing effect on the ideal mode contribution (λ_h), but a destabilizing effect with respect to the ρ_s and d_e terms. The quasilinear enhancement of ω_{*i} ($\alpha > 1$), on the other hand, is of course stabilizing for both. Thus, the two effects are additive (and stabilizing) with respect to the ideal mode but tend to cancel in the case of the reconnecting mode terms. This may account for the rough correlation of nonlinear stability in the simulations with the linear condition with $\lambda_h = 0$.

In the above approximation, ϕ_0 introduces only a shift in the real frequency of the mode, and so does not effect the stability condition. Indeed, ϕ_0 is generally found to make only a weak stabilizing contribution to the stability boundary discussed above. Also, note from Eq. (19) that ω_{*e} can enter the stability condition only through the ρ_s, d_e terms (that is, the ideal mode is sensitive to ω_{*i} only). As a result, the contribution of ω_{*e} to the saturation amplitude is small for ω_{*i} well above the collisionless stability threshold.

IV. CONCLUSION

On the basis of two-fluid MHD simulations, we have confirmed the theoretical prediction[2] that a linearly unstable $m = 1$ mode, in a TFTR-like parameter regime, can saturate in the early nonlinear stage for sufficiently large values of the diamagnetic frequencies $\omega_{*i,e}$. Although this linear mode is predominantly ideal, the saturation process is essentially different from that of the purely ideal $m = 1$ mode,[11] which is inoperative here due to effects that allow magnetic reconnection (e.g., finite electron inertia). Rather, as in the case of the resistive mode,[9] the saturation depends on the presence of $\omega_{*i,e}$ to halt the reconnection.

We find nonlinear effects act in two main ways: (1) they weaken the ideal mode driving term ($\propto \lambda_h$) relative to those of the reconnecting mode ($\propto \rho_s,\ d_e$), and (2) they enhance

the effective values of $\omega_{*i,e}$. These changes lead to a rough correlation between the early-nonlinear stability and the linear $\omega_{*i,e}$-stability condition with $\lambda_h = 0$; $\rho_s, d_e \neq 0$ – *i.e.*, the collisionless reconnecting mode stability condition.

The nonlinear saturation amplitude reached by the mode in the simulations is $\omega_{*i,e}$-dependent: it becomes finite as ω_* falls below the linear stability threshold, and continues to increase monotonically as ω_* is further reduced. The saturation level of the central core displacement ξ_0 can therefore be smaller or larger than, but is typically comparable to, the ideal MHD value[11] $\xi_0 \sim 4.4\lambda_h$. Because the validity of our approach is restricted to the early nonlinear stage ($\xi_0 \ll r_1$), the largest saturation amplitudes considered here are about $\xi_0 \sim (0.25)r_1 \sim 8\lambda_h$, which occur (for the simulated parameters) at $\omega_{*i,e}$ values roughly 1.5 - 2 times above the linear, $\lambda_h = 0$ stability limit. Thus, although the nonlinear amplitudes at these extreme ω_* values increase quite rapidly for decreasing ω_*, no particular value of ω_* can be clearly identified which defines a transition from nonlinear stability to instability. This is in obvious contrast to linear theory, and also possibly experiments, as discussed further below.

The saturated configuration contains an $m = 1$ island of length $l \sim \pi r_1$ and width $w \sim c_0\xi_0$, where $c_0 \sim 1$ for $\xi_0 \sim 4\lambda_h$ or smaller, and $c_0 \sim 2$ for $\xi_0 \gg \lambda_h$. Due to small diffusion effects present in the model, this island can continue to evolve after saturation on a very slow timescale $\tau > 100/\gamma_{lin}$. The behavior of the saturated mode in TFTR over such timescales is erratic and complex. In view of the many effects not considered in this analysis, and the physical uncertainties in the diffusion terms, here we will leave this long-term behavior as an unresolved issue.

Fourier analyses of perturbations in the simulated potentials p, ψ and ϕ at saturation show the $m = n = \pm 1$ and $m = n = 0$ harmonics are dominant. The latter, $m = n = 0$ perturbations were shown to arise from quadratic interactions of the $m = n = 1$ and $m = n = -1$ modes, and represent localized enhancements of the pressure gradient, magnetic shear, and poloidal flow in the singular layer. A quasilinear analysis indicates these enhancements alone can stabilize the $m = n = \pm 1$ modes, and lead to saturation amplitudes in reasonable

agreement with the simulations.

As shown in Ref. 1, sawtooth stability in TFTR is reasonably well described by the linear, reconnecting mode (i.e., $\lambda_h = 0$; $\rho_s, d_e \neq 0$) ω_*-stability condition. As explained above, however, saturation in the early nonlinear stage is found here only for ω_*-values somewhat above this level. Also, the saturation amplitudes predicted by the simulations are typically larger than those observed in experiments (where, e.g., $\xi_0 \sim 1 - 2$ cm). This failure of the simlations to more closely reproduce the observed stability condition and $m = 1$ mode saturation amplitudes in TFTR seems to indicate stabilizing factors outside the present, simplified model are important. A possible explanation is that trapped particle effects, or some other stabilizing effects, act to reduce the effective value of λ_h, thereby reducing the gap between the observed stability and linear theory. Further work is needed to determine the contribution of these and other physically realistic factors.

ACKNOWLEDGMENTS

The authors gratefully acknowledge the useful comments of T. Antonsen, J. Drake and R. Kleva, who also helped in the development of the simulation code used in this study.

This work was supported by the U.S. Department of Energy Contract No. DE-AC02-76-CHO-3073.

APPENDIX: $M = 1$ QUASILINEAR EQUATIONS

With $\nabla^2 \simeq \partial_x^2$, the vorticity equation (1) may be integrated once over x with the result

$$\dot{\phi}_{,x} + [\phi - \tau p, \phi_{,x}] = [\psi, \psi_{,x}] - [\psi, \psi_{,x}]_{x_\infty} \tag{A1}$$

for some $x_\infty \sim x_l \gg \lambda_h$. The x_∞ term may be written as

$$[\psi, \psi_{,x}] = -i\psi_{0,x}^2 \partial_x \left(\psi_1/\psi_{0,x}\right) \tag{A2}$$

$$\approx -i\frac{2\lambda_h}{\pi}\left(\frac{\psi_1}{\psi_{0,x}}\right)_{x_\infty}, \quad x \to x_\infty \tag{A3}$$

$$= -\frac{2\lambda_h}{\pi}\left(\phi_1/\Gamma\right)_{x_\infty}, \tag{A4}$$

where the second line follows from the definition of $\lambda_h = -\pi/\Delta_1'$. The third line follows from the pressure equation (3) and Ohm's law (2) neglecting η, d_e, ρ_s (valid for large x), which yield $p_1 \approx -i\Omega_{*e}\phi_1/\Gamma$ and $\psi_1 \approx -i\psi_{0,x}\phi_1/\Gamma$. In detail, the pressure equation, eliminating $[\psi, J]$ with Eq. (1), can be written as

$$p_1 = -i\Omega_{*e}\phi_1/\Gamma + \frac{\rho_s^2}{(1+\tau)\Gamma}\partial_x\left((\Gamma - i\Omega_{*i})\phi_{1,x} + i\phi_{0,xx}(\phi_1 - \tau p_1)\right) \tag{A5}$$

$$\simeq -i\Omega_{*e}\phi_1/\Gamma + \frac{\rho_s^2}{(1+\tau)\Gamma}\partial_x\left((\Gamma - i\Omega_{*i})(\phi_{1,x} + i\phi_{0,xx}\phi_1/\Gamma)\right) \tag{A6}$$

$$= -i\Omega_{*e}\phi_1/\Gamma + \frac{\rho_s^2}{(1+\tau)\Gamma}\partial_x\left(\lambda^2\partial_x(\phi_1/\Gamma)\right), \tag{A7}$$

where $p_1 \simeq -i\Omega_{*e}\phi_1/\Gamma + O(\rho_s^2/\lambda_h^2)$ was used in the quasilinear correction term $\propto \phi_{0,xx}p_1$ in the second line, leading to an error of $O(\rho_s^4/\lambda_h^4)$. Substituting this result for p_1 into Ohm's law (2) gives

$$\frac{\psi_1}{\psi_{0,x}} = -i\frac{\phi_1}{\Gamma} + i\frac{\lambda_s^2}{\lambda^2}\partial_x\left(\lambda^2\partial_x\left(\frac{\phi_1}{\Gamma}\right)\right) + \frac{\eta\psi_{1,xx}/\psi_{0,x}}{\Gamma + i(\Omega_{*e} - \Omega_{*i})} + \frac{d_e^2(\Gamma - i\Omega_{*i})}{\Gamma + i(\Omega_{*e} - \Omega_{*i})}\left(\frac{\psi_{1,xx}}{\psi_{0,x}} + i\frac{\phi_1}{\Gamma}\frac{\psi_{0,xxx}}{\psi_{0,x}}\right). \tag{A8}$$

Neglecting quasilinear correction terms of order $d_e^2\rho_s^2/\lambda_h^4$, we may take $i\phi_1/\Gamma \simeq -\psi_1/\psi_{0,x}$ in the d_e^2 term above, in which case

$$\frac{\psi_{1,xx}}{\psi_{0,x}} + i\frac{\phi_1}{\Gamma}\frac{\psi_{0,xxx}}{\psi_{0,x}} \simeq \frac{\psi_{1,xx}}{\psi_{0,x}} - \frac{\psi_1}{\psi_{0,x}}\frac{\psi_{0,xxx}}{\psi_{0,x}} = \frac{1}{\psi_{0,x}^2}\partial_x\left(\psi_{0,x}^2\partial_x\left(\frac{\psi_1}{\psi_{0,x}}\right)\right). \tag{A9}$$

Indeed, it is seen to be consistent with the earlier assumption $\nabla^2 \simeq \partial_x^2$ to completely neglect the ϕ_1 term in the above compared to $\psi_{1,xx}/\psi_{0,x}$, in which case that expression may also be used in the η term. As a result, Eq. (A8) becomes:

$$\frac{\psi_1}{\psi_{0,x}} = -i\frac{\phi_1}{\Gamma} + i\frac{\lambda_s^2}{\lambda^2}\partial_x\left(\lambda^2\partial_x\left(\frac{\phi_1}{\Gamma}\right)\right) + \frac{\lambda_e^2}{\psi_{0,x}}\partial_x\left(\psi_{0,x}^2\partial_x\left(\frac{\psi_1}{\psi_{0,x}}\right)\right). \tag{A10}$$

The final result, Eq. (19), is obtained by operating on the above with ∂_x, and using the (integrated) vorticity equation (A1) to eliminate $\partial_x\left(\psi_1/\psi_{0,x}\right)$. The latter equation, replacing p_1 with Eq. (A7), can be written as

$$\lambda^2 \partial_x(\phi_1/\Gamma) = -i\psi_{0,x}^2 \partial_x \left(\psi_1/\psi_{0,x}\right) + \frac{2\lambda_h}{\pi} \left(\phi_1/\Gamma\right)_{x_\infty} \tag{A11}$$

or equivalently

$$\partial_x \left(\psi_1/\psi_{0,x}\right) = i\frac{1}{\psi_{0,x}^2} \left(\lambda^2 Z - \frac{2\lambda_h}{\pi} \int_0^\infty Z dx\right). \tag{A12}$$

REFERENCES

[1] F. M. Levinton, L. Zakharov, S. H. Batha, J. Manickam, M. C. Zarnstorff, Phys. Rev. Lett. **72**, 2895 (1994).

[2] L. Zakharov, F. M. Levinton, S. H. Batha, R. Budny, M. C. Zarnstorff, S. Migliuolo, B. Rogers, *Plasma Phys. and Contr. Nucl. Fus. Res., Proc. 15th Int. Conf., Seville, Spain 1994*, Vienna

[3] K. McGuire, V. Arunasalam, C.W. Barnes, M.G. Bell, M. Bitter, R. Boivin, N.L. Bretz, R. Budny, C.E. Bush, A. Cavallo, T.K. Chu, S.A.Cohen, P. Colestock, S.L. Davis, D.L. Dimock, H.F. Dylla, P.C. Efthimion, A.B. Ehrhardt, R.J. Fonck, E.D. Fredrickson, H.P. Furth, G. Gammel, R.J. Goldston, G.J. Greene, B. Grek, L.R. Grisham, G.W. Hammett, R.J. Hawryluk, H.W. Hendel, K.W. Hill, E. Hinnov, D.J. Hoffman, J.C. Hosea, R.B. Howell, H. Hsain, R.A. Hulse, A.C. Janos, D.L. Jassby, F.C. Jobs, D.W. Johnson, L.C. Johnson, R. Kaita, C. Kieras–Phillips, S.J. Kilpatrick, P.H. Lamarche, B. LeBlanc, D. Manos, D.K. Mansfield, E. Mazzucato, M.P. McCarthy, D.C. McCune, D.H. McNeill, D.M. Meade, S.S. Medley, D.R. Mikkelsen, D.A. Monticello, R.W. Motley, D. Mueller, J. Murphy, Y. Nagayama, R. Nazikian, E.B. Neischmidt, D.K. Owens, H.K. Park, W. Park, S. Pitcher, A.T. Ramsey, M.H. Redi, A.L. Roquemore, P.H. Rutherford, G. Schilling, J. Schivell, G.L. Schmidt, S.D. Scott, J. Sinnis, J.E. Stevens, B.C. Stratton, W. Stodiek, E.J. Synakowski, W. M. Tang, G. Taylor, J.I. Timberlake, H.H. Towner, M. Ulrickson, S. von Goeler, R.M. Wieland, M. Williams, J.R. Wilson, K.L. Wong, M. Yamada, S. Yoshikawa, K.M. Young, M.C. Zarnstorff, S.J. Zweben, Phys. Fluids **B 2**, 1287 (1990).

[4] M. N. Bussac, R. Pellat, D. Edery, J. L. Soule, Phys. Rev. Lett. **35**, 1638 (1975).

[5] F. Porcelli, Phys. Rev. Lett. **66**, 425 (1991).

[6] L. Chen, R. B. White, M. N. Rosenbluth, Phys. Rev. Lett. **52**, 1122 (1984).

[7] T. M. Antonsen Jr., A. Bondeson, Phys. Rev. Lett. **71**, 2046 (1993).

[8] Y. Zhao, R. B. White, private communication (1994).

[9] D. Biskamp, Phys. Rev. Lett. B **46**, 1522 (1981).

[10] D. Biskamp, J. F. Drake, Phys. Rev. Lett. B **73**, 971 (1994).

[11] M. N. Rosenbluth, R. Y. Dagazian, P. H. Rutherford, Phys. Fluids **16**, 1894 (1973).

[12] F. L. Waelbroeck, Phys. Fluids B **1**, 2372 (1989).

[13] L. Zakharov, B. Rogers, S. Migliuolo, Phys. Fluids B **5**, 2498 (1993).

[14] R. D. Hazeltine, C. T. Hsu, P. J. Morrison, Phys. Fluids **30**, 3204 (1987).

[15] A. Y. Aydemir, Phys. Fluids B **3**, 3025 (1991).

[16] L. Zakharov, B. Rogers, Phys. Fluids B **4**, 3285 (1992).

[17] J. F. Drake, R. G. Kleva, Phys. Rev. Lett. **66**, 1458 (1991).

[18] M. Ottaviani, F. Porcelli, Phys. Rev. Lett. **71**, 3802 (1993).

[19] J. F. Drake, J. Gerber, R. G. Kleva, J. Geophys. Res. **99**, 11211 (1994).

[20] D. Biskamp, Phys. Fluids B **3**, 3353 (1991).

[21] B. Coppi, R. Galvo, R. Pellaat, M. Rosenbluth, P. Rutherford, Sov. J. Plasma Phys. **2**, 533 (1976), [Fiz. Plasmy **2**, 961 (1976)].

[22] R. D. Hazeltine, J. D. Meiss, Phys. Rep. **121**, 90 (1985).

[23] G. Ara, B. Basu, B. Coppi, G. Laval, M. N. Rosenbluth, B. V. Waddell, Ann. Phys. (NY) **112**, 443 (1978).

FIGURES

FIG. 1. A sketch of the simulated "layer region" containing the $m = 1$ island and reconnection layer.

FIG. 2. ξ $(= \xi/r_1)$ vs t $(= t/\tau_A^*)$ for $\omega_* = 0$ (upper curve) and $\omega_{*i}(= \omega_{*i}\tau_A^*) = -\omega_{*e} = 0.054$ (lower curve).

FIG. 3. Same as the $\omega_* \neq 0$ case in Fig. 2 (shown as dashed line) except $\mu = \mu_e = \kappa = 3 \times 10^{-6}$.

FIG. 4. Approximate saturation amplitudes obtained from simulations: (1) asterisks: $\rho = 1$, $\rho_s(= \rho_s/r_1) = 0.015$; (2) triangles: $r = 3$, $\rho_s = 0.015$; (3) squares: $r = 3$, $\rho_s = 0.03$. Also, dashed line is analytic result for $r = 1$, $\rho_s = 0.015$ from Eq. (24).

FIG. 5. (a) Contours of ψ at $t = 400$ of $\omega_* \neq 0$ case in Fig. 2 ($x = x/r_1$, $z = z/r_1$). (b) Contours of $J = \nabla^2\psi$ at $t = 400$.

FIG. 6. (a) Fourier transform of ϕ for $|m| = 1, 0, 2, 3$ at $t = 400$ (descending order, $x < 0.01$). Curves show $|\phi_m| + |\phi_{-m}| = 2|\phi_m|$ for $m \neq 0$ and $|\phi_0|$ for $m = 0$. (b) Fourier transform of $p - p^{(0)}$ for $|m| = 1, 0, 2, 3$ at $t = 400$, displayed as in Fig. 6a. (c) Fourier transform of $\psi - \psi^{(0)}$ for $|m| = 1, 0, 2, 3$ at $t = 400$, displayed as in Fig. 6a.

FIG. 7. (a) The $m = 0$ harmonic of ϕ' vs x at $t = 400$ from simulation (solid line) and unperturbed, $t = 0$ profile (dashed line). (b) The $m = 0$ harmonic of p' vs x at $t = 400$ from simulation (solid line) and unperturbed, $t = 0$ profile (dashed line). (c) The $m = 0$ harmonic of ψ' vs x at $t = 400$ from simulation (solid line) and unperturbed, $t = 0$ profile (dashed line).

FIG. 8. (a) ϕ_0 vs x $(= x/r_1)$ at $t = 400$ from simulation (solid line) and from analytic expression in Eq. (28) (dashed line). (b) $p_0 - p_0^{(0)}$ vs x at $t = 400$ from simulation (solid line) and from analytic expression in Eq. (28) (dashed line). (c) $\psi_0 - \psi_0^{(0)}$ vs x at $t = 400$ from simulation (solid line) and from analytic expression in Eq. (28) (dashed line).

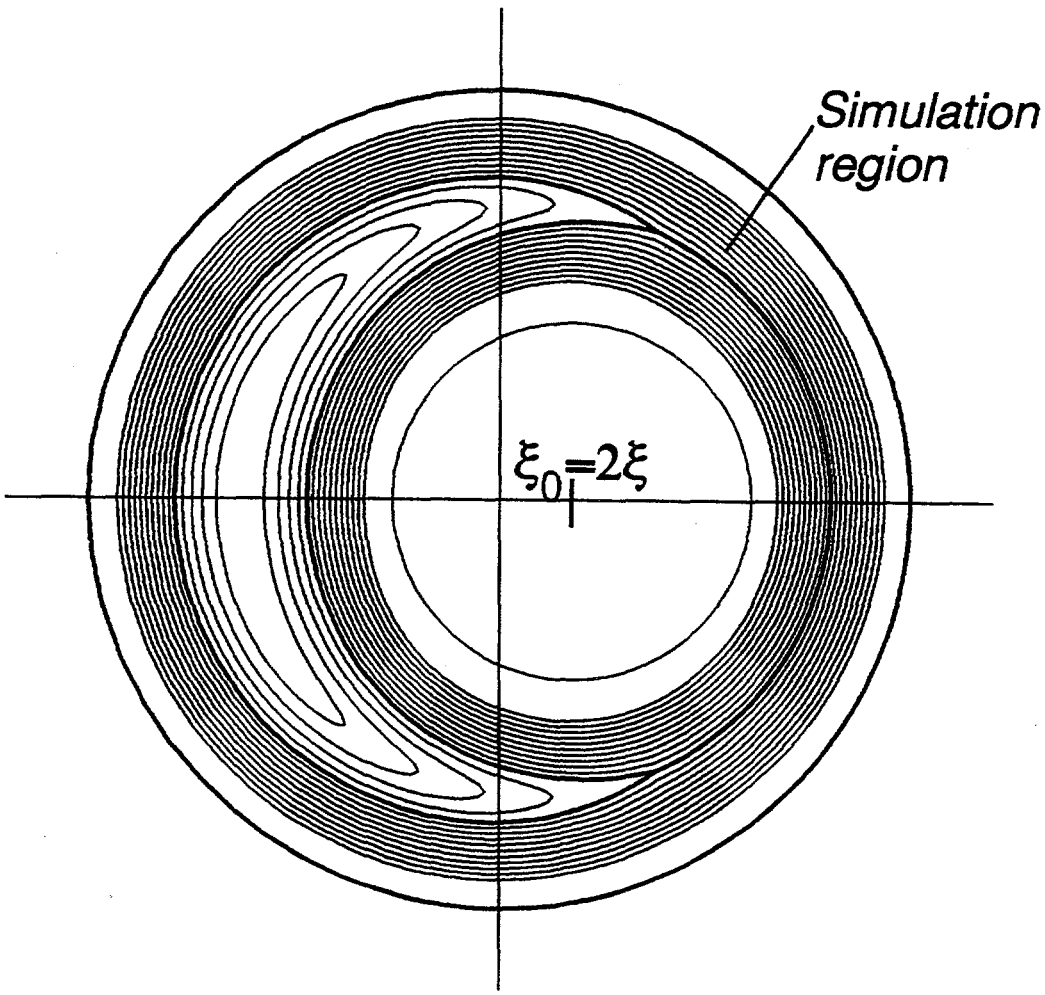

Fig. 1

Fig. 2

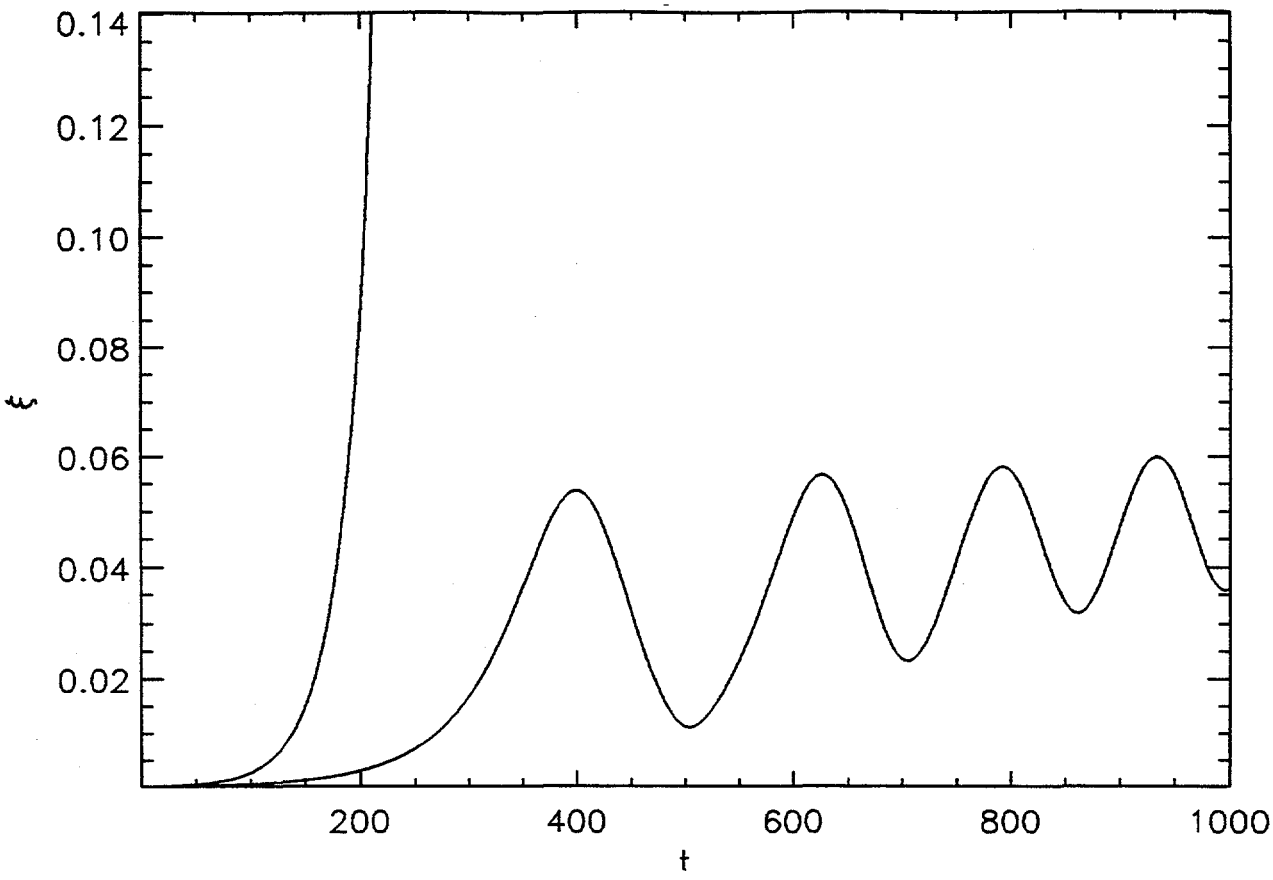
0.14
0.12
0.10
0.08
0.06
0.04
0.02
ε
200
400
600
800
1000
t

Fig. 3

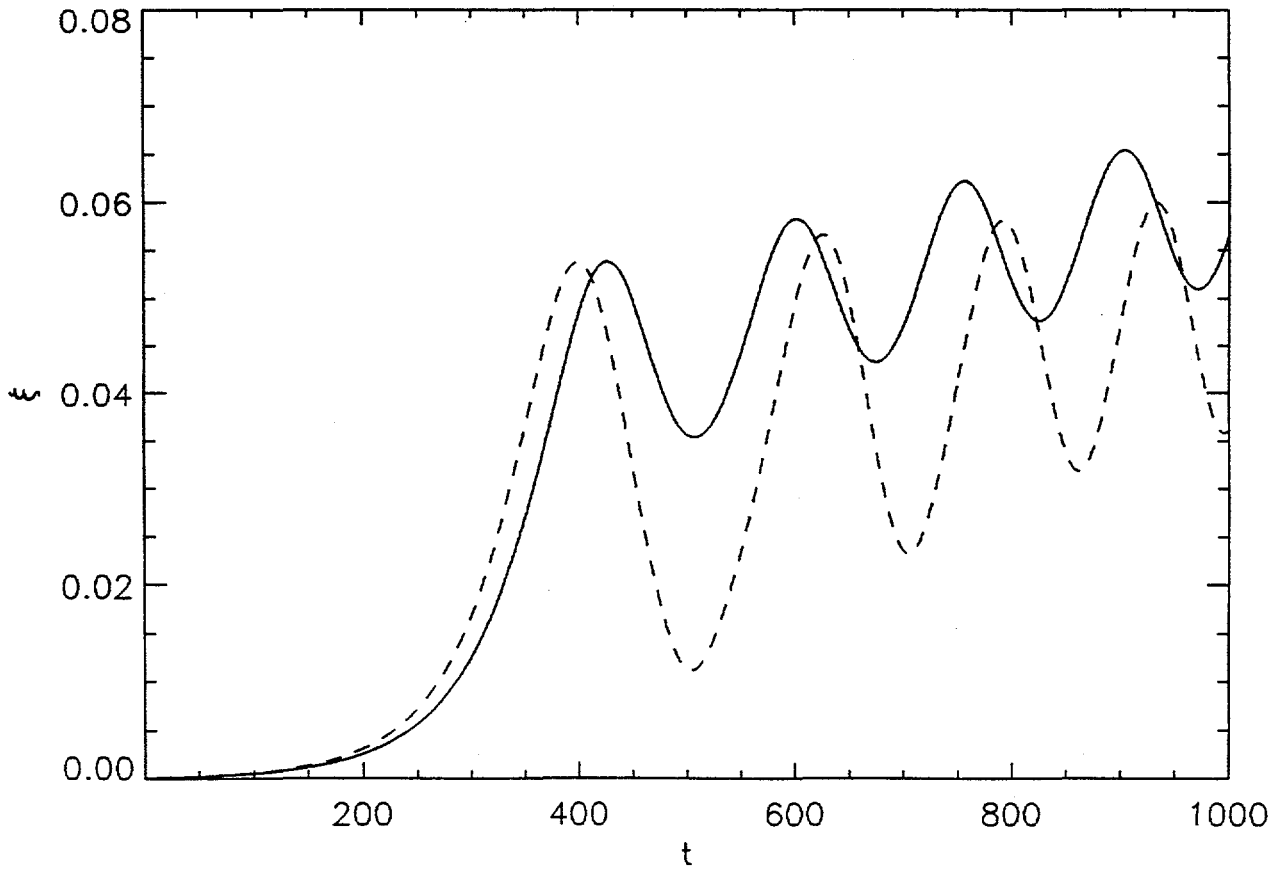
0.08
0.06
0.04
0.02
0.00
ε
200
400
600
800
1000
t

Fig. 4

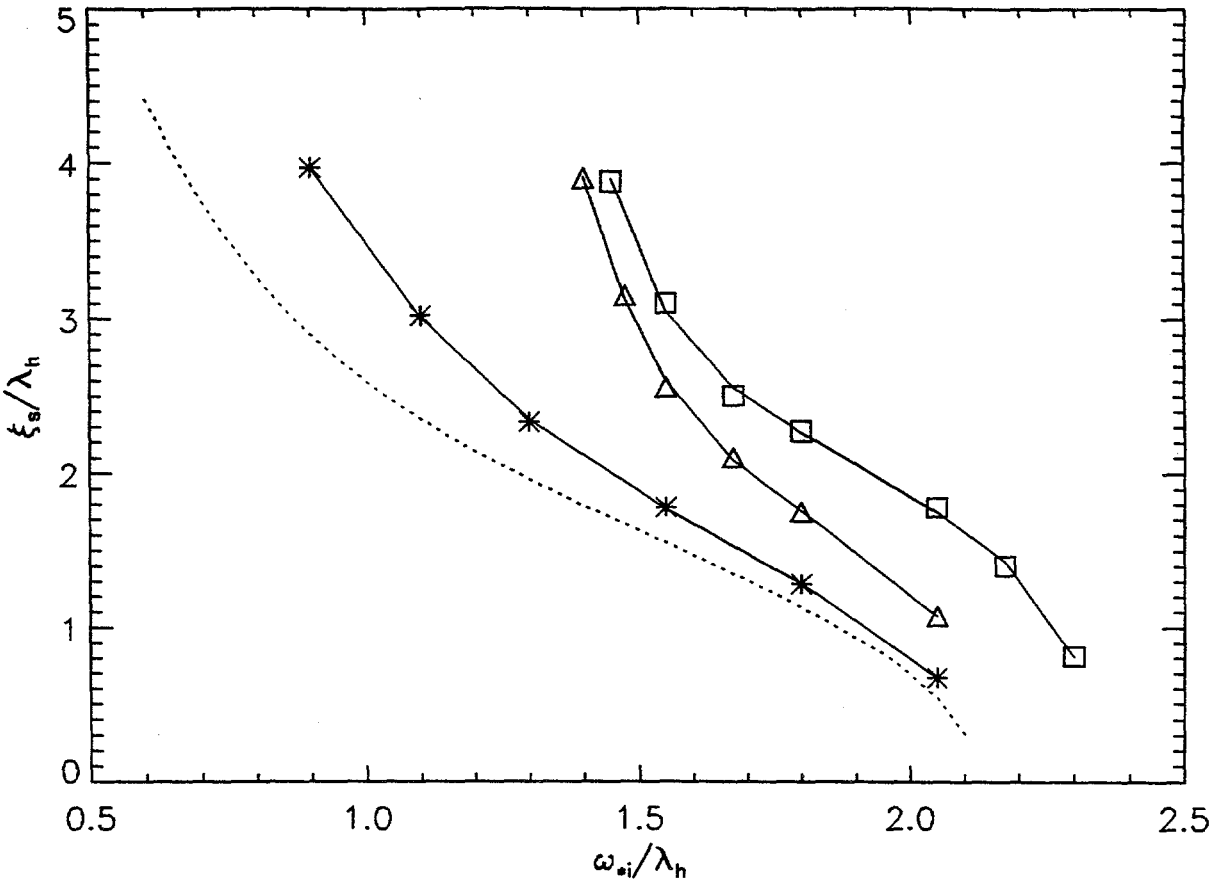

Fig. 5a

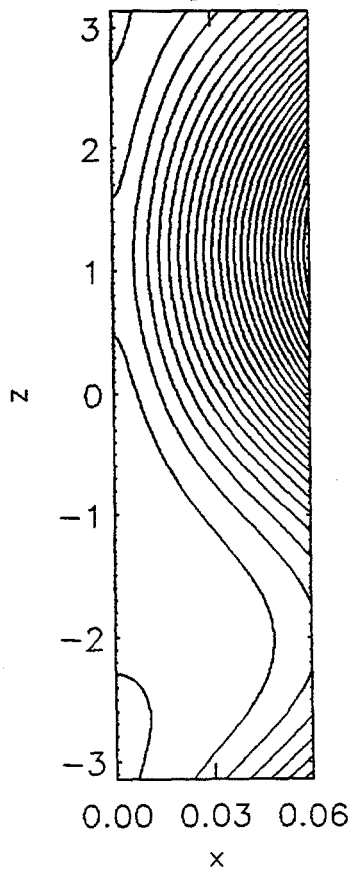

Fig. 5b

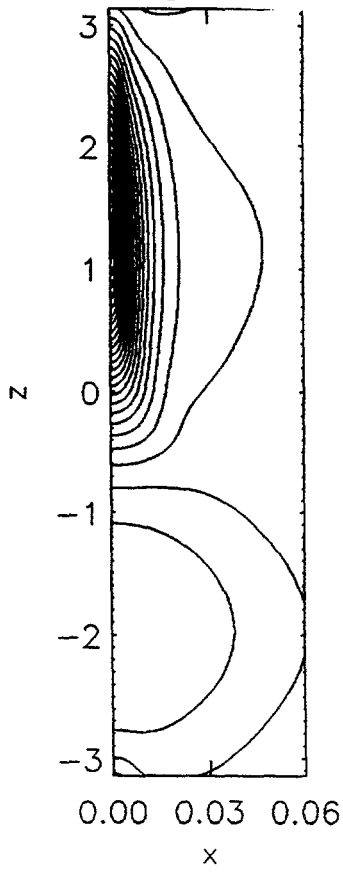

Fig. 6a

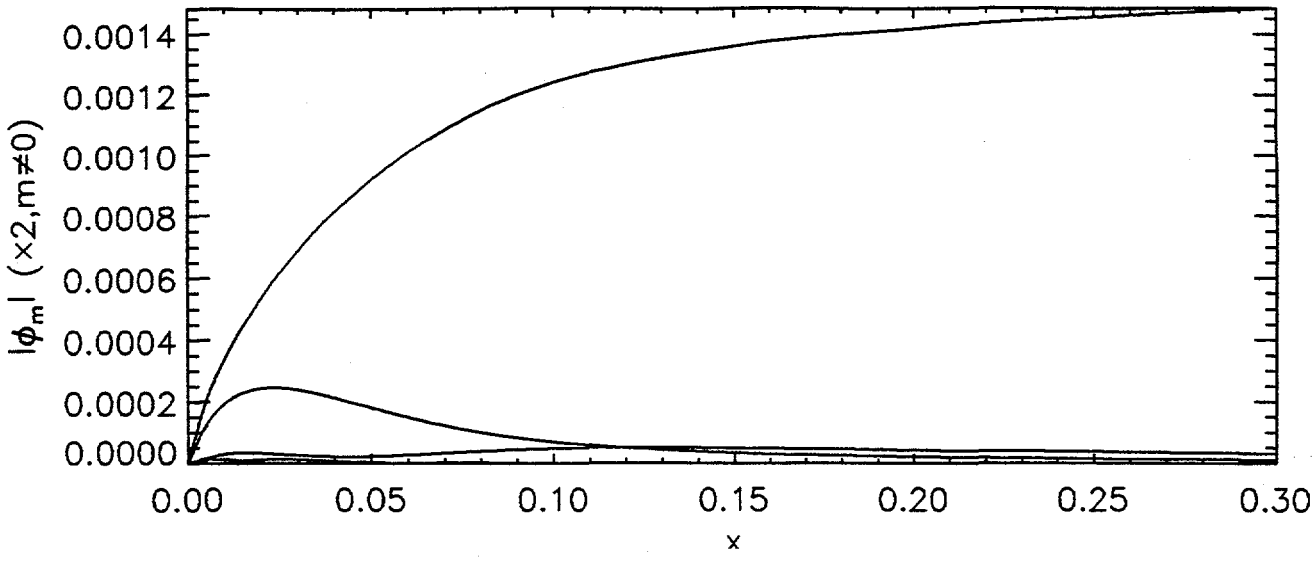

Fig. 6b

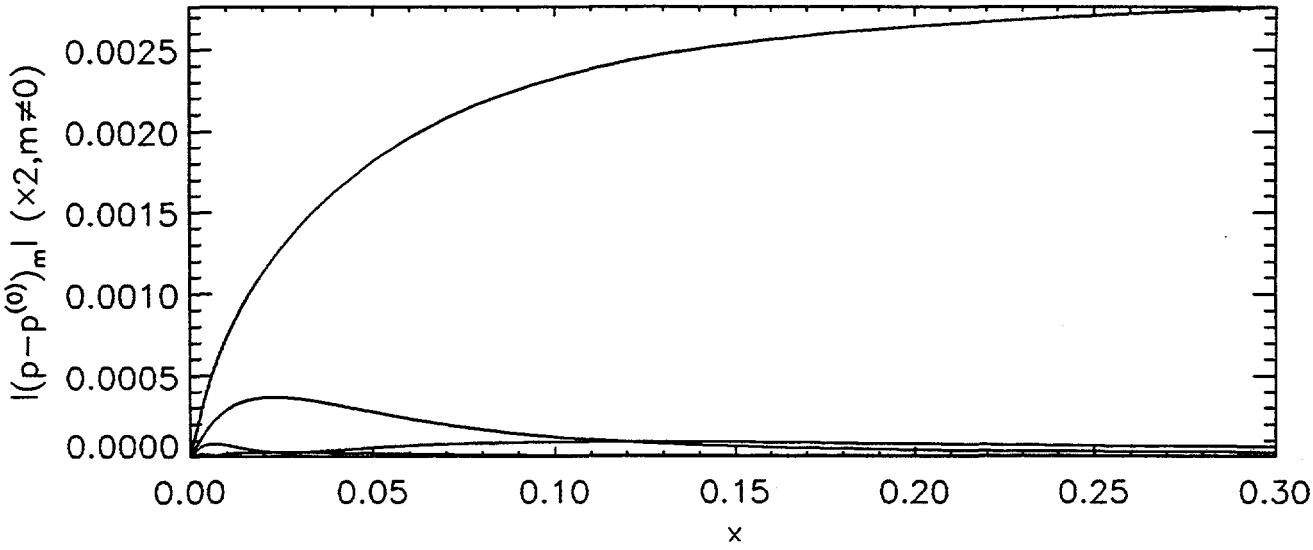

Fig. 6c

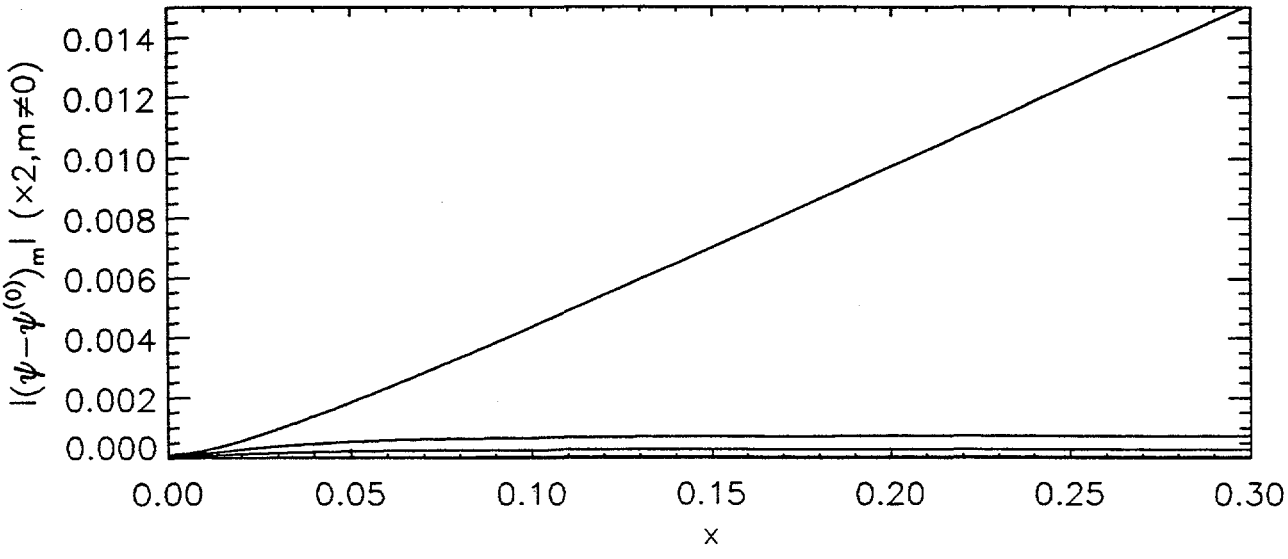

Fig. 7a

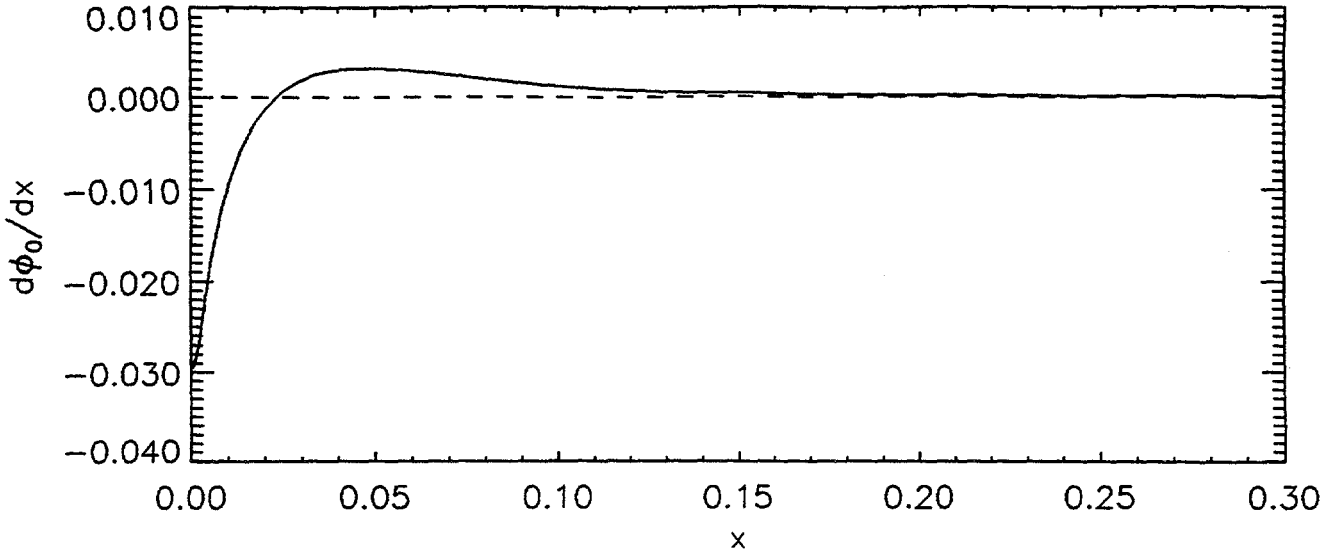

Fig. 7b

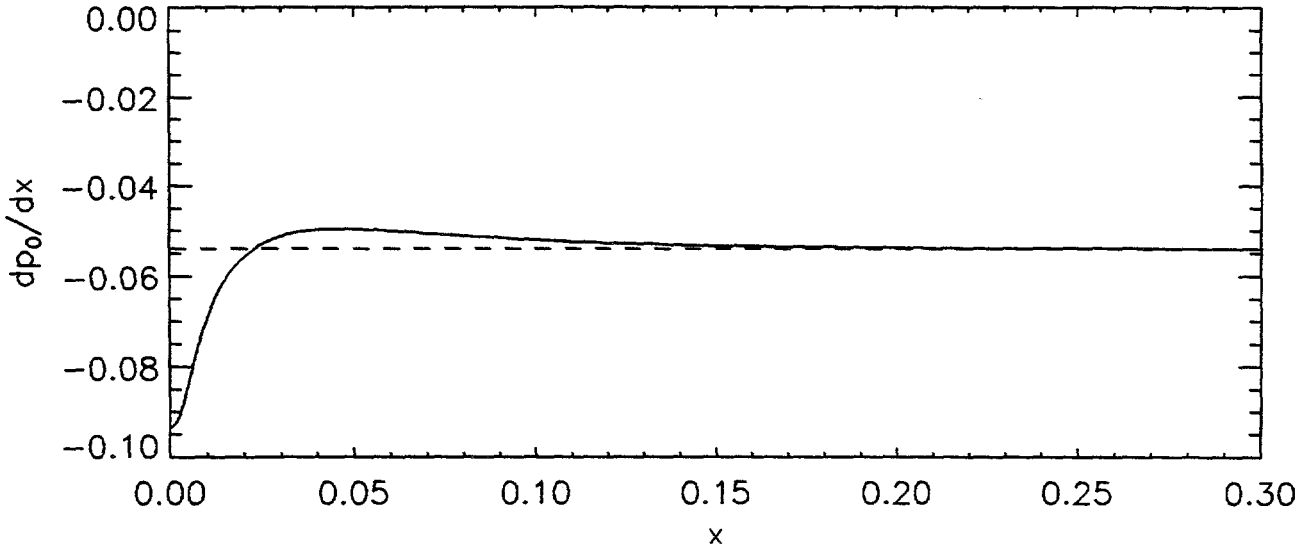

Fig. 7c

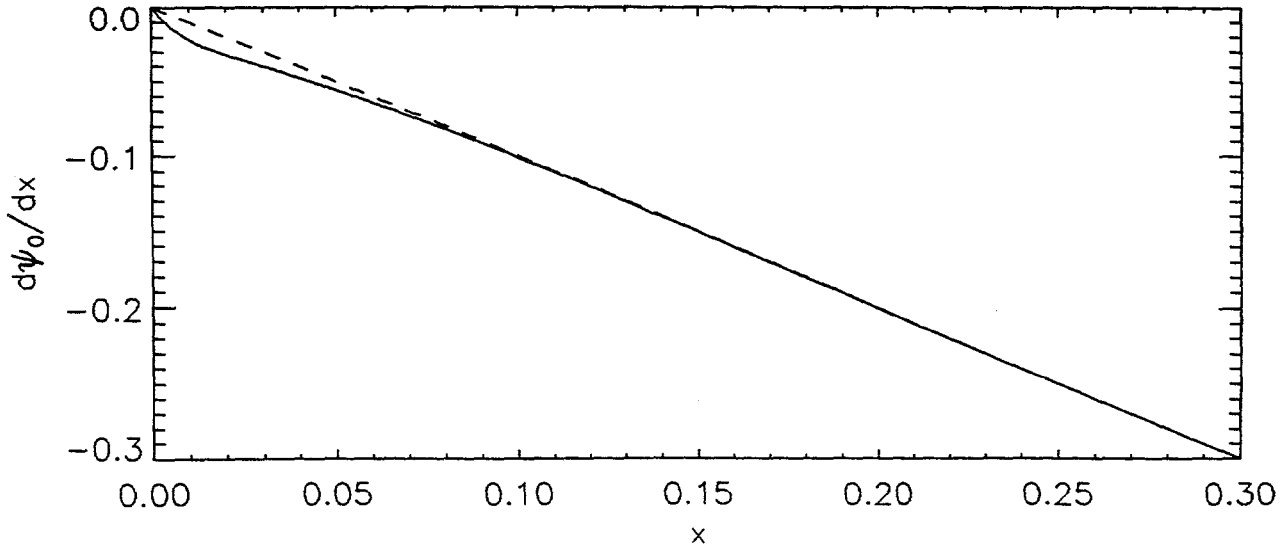

Fig. 8a

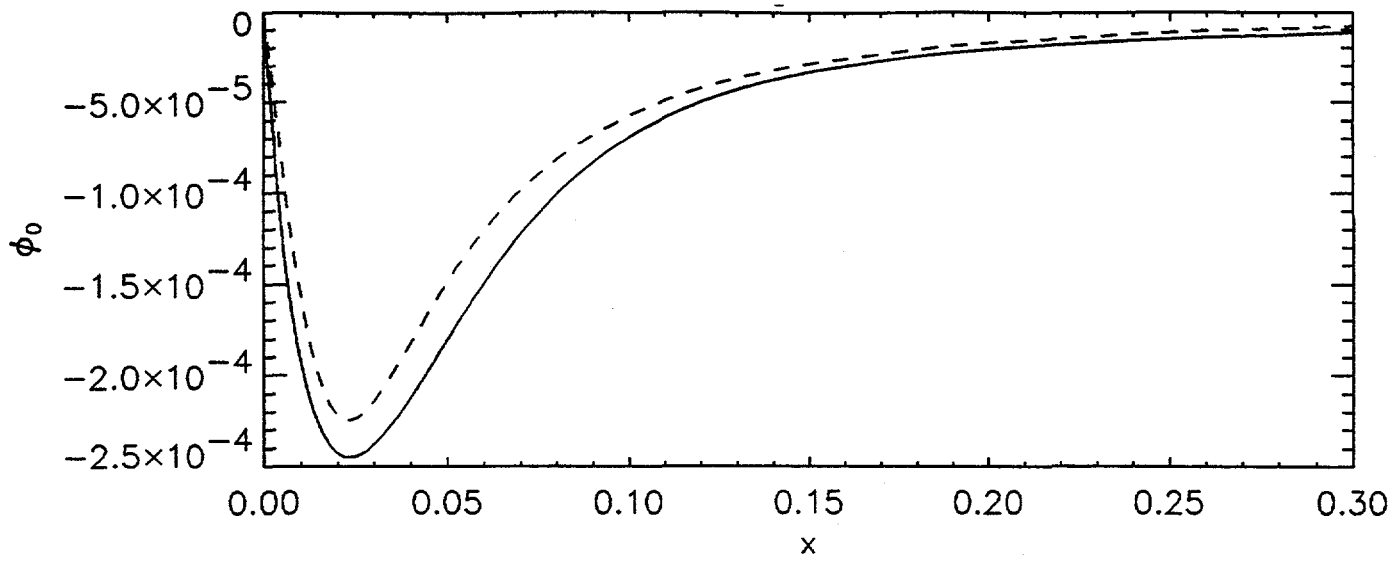

Fig. 8b

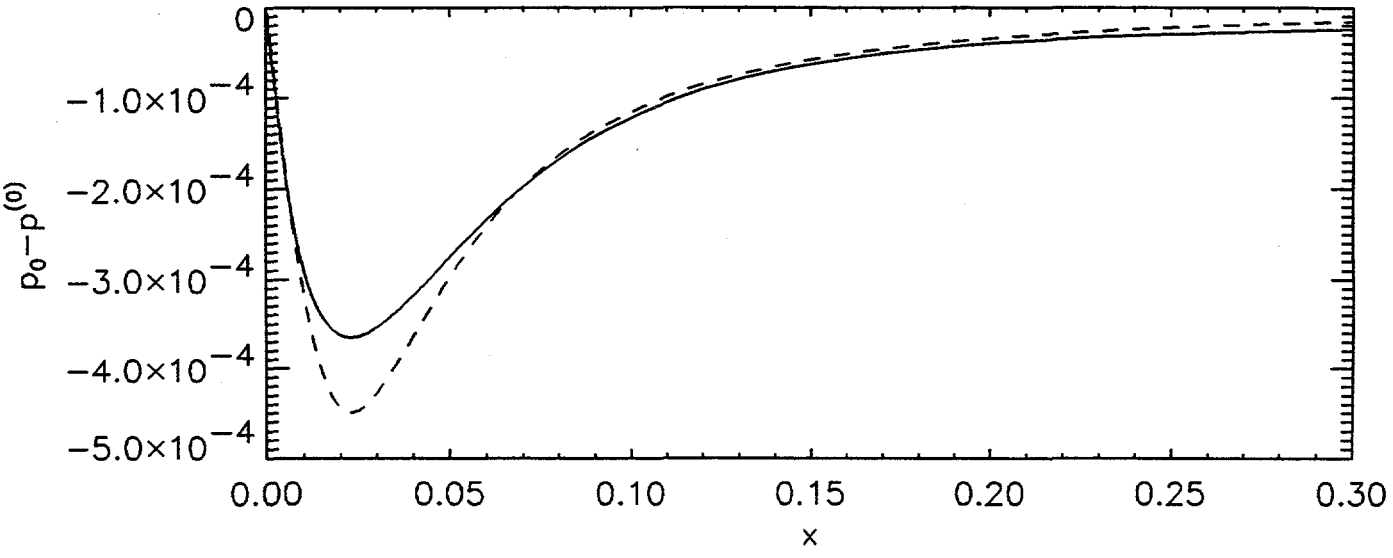

Fig. 8c

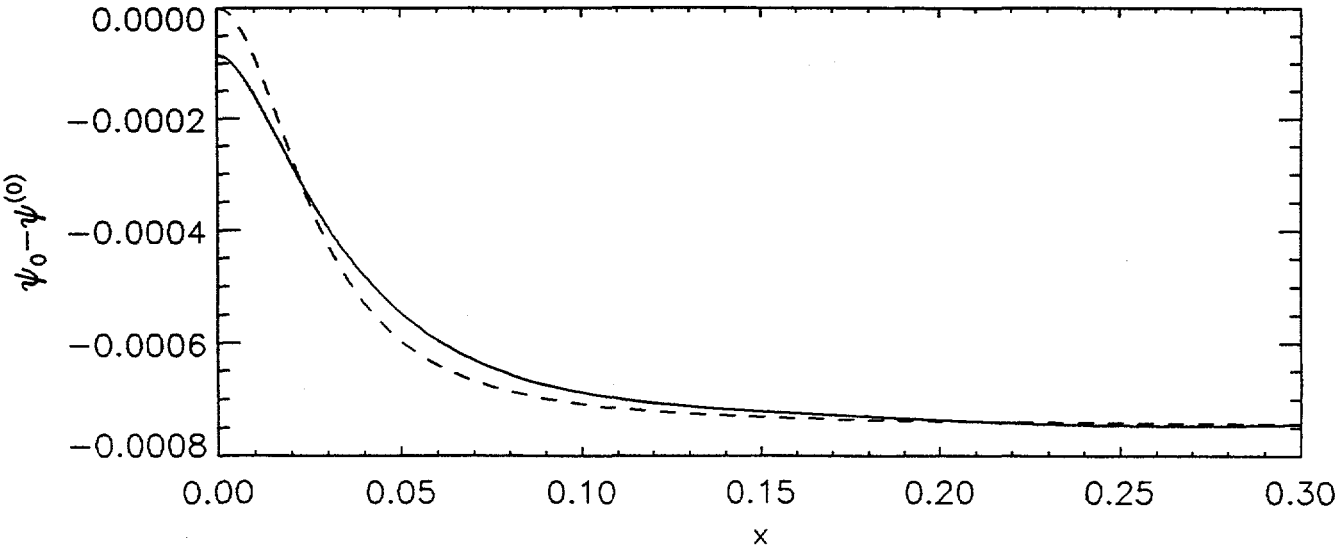

EXTERNAL DISTRIBUTION IN ADDITION TO UC-420

Dr. F. Paoloni, Univ. of Wollongong, AUSTRALIA
Prof. R.C. Cross, Univ. of Sydney, AUSTRALIA
Plasma Research Lab., Australian Nat. Univ., AUSTRALIA
Prof. I.R. Jones, Flinders Univ, AUSTRALIA
Prof. F. Cap, Inst. for Theoretical Physics, AUSTRIA
Prof. M. Heindler, Institut für Theoretische Physik, AUSTRIA
Prof. M. Goossens, Astronomisch Instituut, BELGIUM
Ecole Royale Militaire, Lab. de Phy. Plasmas, BELGIUM
Commission-European, DG. XII-Fusion Prog., BELGIUM
Prof. R. Boucique, Rijksuniversiteit Gent, BELGIUM
Dr. P.H. Sakanaka, Instituto Fisica, BRAZIL
Prof. Dr. I.C. Nascimento, Instituto Fisica, Sao Paulo, BRAZIL
Instituto Nacional De Pesquisas Espaciais-INPE, BRAZIL
Documents Office, Atomic Energy of Canada Ltd., CANADA
Ms. M. Morin, CCFM/Tokamak de Varennes, CANADA
Dr. M.P. Bachynski, MPB Technologies, Inc., CANADA
Dr. H.M. Skarsgard, Univ. of Saskatchewan, CANADA
Prof. J. Teichmann, Univ. of Montreal, CANADA
Prof. S.R. Sreenivasan, Univ. of Calgary, CANADA
Prof. R. Marchand, INRS-Energie et Materiaux, CANADA
Dr. R. Bolton, Centre canadien de fusion magnétique, CANADA
Dr. C.R. James,, Univ. of Alberta, CANADA
Dr. P. Lukác, Komenského Universzita, CZECHO-SLOVAKIA
The Librarian, Culham Laboratory, ENGLAND
Library, R61, Rutherford Appleton Laboratory, ENGLAND
Mrs. S.A. Hutchinson, JET Library, ENGLAND
Dr. S.C. Sharma, Univ. of South Pacific, FIJI ISLANDS
P. Mähönen, Univ. of Helsinki, FINLAND
Prof. M.N. Bussac, Ecole Polytechnique,, FRANCE
C. Mouttet, Lab. de Physique des Milieux Ionisés, FRANCE
J. Radet, CEN/CADARACHE - Bat 506, FRANCE
Prof. E. Economou, Univ. of Crete, GREECE
Ms. C. Rinni, Univ. of Ioannina, GREECE
Preprint Library, Hungarian Academy of Sci., HUNGARY
Dr. B. DasGupta, Saha Inst. of Nuclear Physics, INDIA
Dr. P. Kaw, Inst. for Plasma Research, INDIA
Dr. P. Rosenau, Israel Inst. of Technology, ISRAEL
Librarian, International Center for Theo Physics, ITALY
Miss C. De Palo, Associazione EURATOM-ENEA , ITALY
Dr. G. Grosso, Istituto di Fisica del Plasma, ITALY
Prof. G. Rostangni, Istituto Gas Ionizzati Del Cnr, ITALY
Dr. H. Yamato, Toshiba Res & Devel Center, JAPAN
Prof. I. Kawakami, Hiroshima Univ., JAPAN
Prof. K. Nishikawa, Hiroshima Univ., JAPAN
Librarian, Naka Fusion Research Establishment, JAERI, JAPAN
Director, Japan Atomic Energy Research Inst., JAPAN
Prof. S. Itoh, Kyushu Univ., JAPAN
Research Info. Ctr., National Instit. for Fusion Science, JAPAN
Prof. S. Tanaka, Kyoto Univ., JAPAN
Library, Kyoto Univ., JAPAN
Prof. N. Inoue, Univ. of Tokyo, JAPAN
Secretary, Plasma Section, Electrotechnical Lab., JAPAN
Dr. O. Mitarai, Kumamoto Inst. of Technology, JAPAN
Dr. G.S. Lee, Korea Basic Sci. Ctr., KOREA
J. Hyeon-Sook, Korea Atomic Energy Research Inst., KOREA
D.I. Choi, The Korea Adv. Inst. of Sci. & Tech., KOREA
Leandro Melendez Lugo, Inst. Nac'l. de Inves. Nucl, MEXICO
Prof. B.S. Liley, Univ. of Waikato, NEW ZEALAND
Inst of Physics, Chinese Acad Sci PEOPLE'S REP. OF CHINA
Library, Inst. of Plasma Physics, PEOPLE'S REP. OF CHINA
Tsinghua Univ. Library, PEOPLE'S REPUBLIC OF CHINA
Z. Li, S.W. Inst Physics, PEOPLE'S REPUBLIC OF CHINA
Prof. J.A.C. Cabral, Instituto Superior Tecnico, PORTUGAL
Prof. M.A. Hellberg, Univ. of Natal, S. AFRICA
Prof. D.E. Kim, Pohang Inst. of Sci. & Tech., SO. KOREA
Prof. C.I.E.M.A.T, Fusion Division Library, SPAIN
Dr. L. Stenflo, Univ. of UMEA, SWEDEN
Library, Royal Inst. of Technology, SWEDEN
Prof. H. Wilhelmson, Chalmers Univ. of Tech., SWEDEN
Centre Phys. Des Plasmas, Ecole Polytech, SWITZERLAND
Bibliotheek, Inst. Voor Plasma-Fysica, THE NETHERLANDS
Asst. Prof. Dr. S. Cakir, Middle East Tech. Univ., TURKEY
Dr. V.A. Glukhikh,Sci. Res. Inst. Electrophys.I Apparatus, USSR
Dr. D.D. Ryutov, Siberian Branch of Academy of Sci., USSR
Dr. G.A. Eliseev, I.V. Kurchatov Inst., USSR
Librarian, The Ukr.SSR Academy of Sciences, USSR
Dr. L.M. Kovrizhnykh, Inst. of General Physics, USSR
Kernforschungsanlage GmbH, Zentralbibliothek, W. GERMANY
Bibliothek, Inst. Für Plasmaforschung, W. GERMANY
Prof. K. Schindler, Ruhr-Universität Bochum, W. GERMANY
Dr. F. Wagner, (ASDEX), Max-Planck-Institut, W. GERMANY
Librarian, Max-Planck-Institut, W. GERMANY